Experimental study on shear-dominant fiber failure in CFRP laminates by out-of-plane shear loading

Yashiro, Shigeki
Department of Aeronautics and Astronautics, Kyushu University

Ogi, Keiji
Graduate School of Science and Engineering, Ehime University

出版情報：Journal of Composite Materials. 53 (10), pp.1337-1346, 2019-05-01. American Society for Composites
バージョン：

Journal of Composite Materials 2019, Vol. 53(10) 1337–1346
DOI: 10.1177/0021998318801454

Experimental study on shear-dominant fiber failure in CFRP laminates by out-of-plane shear loading

Shigeki Yashiro [1,*], Keiji Ogi [2]

[1] Department of Aeronautics and Astronautics, Kyushu University

744 Motooka, Nishi-ku, Fukuoka 819-0395, Japan

[2] Graduate School of Science and Technology, Ehime University

3 Bunkyo-cho, Matsuyama, Ehime 790-8577, Japan

* Corresponding author: yashiro@aero.kyushu-u.ac.jp (S. Yashiro)

Abstract

Understanding the shear behavior and resulting fiber failure of fiber-reinforced plastics (FRPs) is required for better prediction of their behavior during the machining process, but knowledge regarding the shear strength of fiber failure is limited. In this study, out-of-plane shear tests were conducted to observe the shear behavior of carbon FRP (CFRP) laminates subjected to high shear stress exceeding the shear strength of matrix failure. The longitudinal fibers in CFRP unidirectional laminates were cut by shear loading without severe internal damage and the maximum shear stress causing progressive fiber breaks was much higher than the shear strength of matrix failure. This result suggested the possibility of out-of-plane shearing as a machining method for FRPs and shear tests were subsequently performed for CFRP cross-ply laminates. Delamination was generated by high shear stress to cut the reinforcing fibers, but

the size of the remaining damage was small even in the thermoset CFRP laminates in which delamination likely occurs, without any optimization of the trimming conditions.

Keywords: fiber-reinforced polymer composites; mechanical testing; shear property; trimming method

1. Introduction

Carbon-fiber-reinforced plastics (CFRPs) have been used in various industries. Material characterization is required for their application to real structures, and in the case of CFRPs with continuous fibers, the in-plane and interlaminar properties have been investigated intensively. As matrix cracks and fiber/matrix debonding are first generated by shear stresses, the shear failure of the reinforcing fibers is less important in the in-service stage. However, in the machining stage (e.g., milling and drilling), fibers are generally cut by shear loading. Matrix and interlaminar shear failure always occurs in well-known shear tests such as the Iosipescu shear test (ASTM D5379); thus, there is scant knowledge regarding the shear properties of fiber failure.

Many experiments and analyses on the machining of composite materials have been reported [1,2]. Information regarding the shear behavior of CFRPs and carbon fibers is essential to clarify effects of the machining processes involving the cutting force, deformation, damage, and chip formation [3,4]. Numerical analyses of orthogonal cutting [5-7] have been performed

to understand the cutting process of reinforcing fibers. The reported numerical simulations can be divided into two groups from the viewpoint of how they model the work material to be cut. One group consists of micro-mechanical modeling studies [8-13], and the other group consists of equivalent homogeneous modeling studies [14-16]. In micro-mechanical modeling, the microstructures of composites, consisting of fibers, matrix and their interface, is represented explicitly and the material degradation of each component is analyzed during machining. This approach predicts fiber breaks, matrix damage, and interfacial debonding as well as subsequent fiber pullout behavior. In equivalent homogeneous modeling, the real inhomogeneous material is replaced by an equivalent orthotropic, homogeneous, single-phase material which incorporates stress-based damage criteria. This approach allows the simulation of continuous chip formation during the machining process. The strength properties used in these studies are listed in Tables 1a and 1b. The lack of shear strength in the micro-mechanical model suggests that fiber failure (cutting) has been evaluated mainly using the longitudinal strength, although most machining methods are driven in the shear mode. Equivalent homogeneous modeling has been employed in drilling simulations [18-22], and the strength properties used in these simulations are listed in Table 1c. The shear strength in the equivalent homogeneous model was derived from the usual shear tests and the material data sheets for matrix failure. Machining phenomena are accompanied by fiber failure owing to shear loading, and the relevant strength property is important to accurately predict this process.

[insert Table 1]

Further, the strength for the shear failure of reinforcing fibers is investigated. Tensile tests of CFRP unidirectional laminates with small off-axis angles (Appendix) suggested that the shear strength of fiber failure was different from the usual shear strength of matrix failure. To the best of the authors' knowledge, there have been few studies suggesting this property. Crescenzi et al. [23] performed the Iosipescu test and the punch-tool shear test (ASTM D732) in a testing campaign of S-2 glass/epoxy composites. The shear strength measured by the punch-tool shear test was 297 MPa, which was different from the results of the Iosipescu test (49–60 MPa). Formisano et al. [24] carried out punch-tool shear testing of glass-fiber-reinforced plastics (GFRP) to understand the shear behavior during machining. They prepared special specimens to achieve constant fiber alignment around the punch. The maximum shear stress accompanied by fiber failure (200 MPa) was five times higher than the shear strength of matrix failure. These studies suggested that the shear strength required to cut the fibers was apparently different from that resulting in matrix failure. However, radial fiber orientation is required to realize uniform fiber orientation around the punch. Therefore, the shear behavior obtained using the punch-tool shear test reflects the effect of fiber shear failure but does not completely reflect the properties of the reinforcements.

Therefore, in this study, the shear behavior of fiber failure is investigated by the out-of-plane shear testing of CFRP laminates. We employed a test method similar to press-shearing to impart

uniform shear deformation to the fibers. The experimental results of the out-of-plane shear testing of CFRP unidirectional laminates are first presented and then the fiber failure caused by the shear loading and the relevant shear strength are discussed. The out-of-plane shear test is similar to machining methods such as punch-shearing and fine blanking, although there have been very few attempts to apply them to FRPs. The feasibility of trimming of CFRPs using out-of-plane shearing is discussed based on the observations of cross-ply laminates.

2. Materials and procedure

The out-of-plane shear tests of CFRP laminates were carried out to investigate the shear strength of fiber failure. Carbon/epoxy composite laminates (T700S/#2592, Toray Industries) were used, and the stacked prepreg sheets were cured at 130 °C under a pressure of 0.2 MPa for 2 hours by using a hot-press machine with a vacuum chamber. Unidirectional laminates ($[0_8]$ and $[90_8]$) were tested to investigate their shear strength (Section 3.1) and cross-ply laminates ($[0_2/90_2]_S$ and $[0/90]_{2S}$) were tested to demonstrate the trimming of CFRP laminates (Section 3.2). Coupon specimens were cut out from the laminates using a diamond saw and each specimen had a length of 40 mm, width of 10 mm, and thickness of 1.1 mm.

Figure 1 illustrates the experimental setup and shows a schematic diagram of the jig used for the out-of-plane shear tests. The upper jig moved along the vertical guide pole with no inclination. The upper and lower dies used to generate shear deformation were flat blocks; more

specifically, the knife angle and shearing angle were both zero. Further, 30 mm of the specimen was fixed on the lower jig using a stopper plate and the remaining 10 mm was cut off. The stopper plate was screwed in place using two bolts with springs between them. The jig was placed on a universal testing machine (AG-50kNXplus, Shimadzu), and the load and crosshead displacement were measured during the test.

[insert Figure 1]

Fiber breakage could be induced by reducing the clearance, i.e., the horizontal distance between the upper and lower dies. The clearance (0.01 to 0.50 mm) was adjusted by inserting thin spacer plates between the lower die and the jig body.

3. Experimental results and discussion

3.1 Fiber failure induced by shear loading

First, transverse specimens with a fiber orientation angle of $\theta = 90°$ were tested at a clearance of 0.05 mm. The resulting shear stress–displacement diagrams are illustrated in Fig. 2a, where the shear stress is the applied load divided by the cross-sectional area and the displacement is the crosshead displacement. The maximum stress was approximately 60 MPa, and its variation was small. This maximum shear stress was consistent with the shear strength estimated by tensile tests of the off-axis unidirectional laminates (see Appendix). It was presumed from these results and punch-tool shear tests [24] that the in-plane shear strength measured using several

test methods is not related to fiber failure. A curvy edge observed in the fixed side coupon (Fig. 2b) was similar to the failure pattern of polymers obtained using the punch-tool shear test [25], and this observation suggested a similarity between these two tests.

[insert Figure 2]

Figure 3 presents typical shear stress–displacement curves of the longitudinal specimens (θ = 0°) at several clearances. The overall shapes of the curves are similar. When the load was removed before reaching the maximum stress, the specimen was bent locally between the upper and lower dies, suggesting plastic deformation and the accumulation of microscopic damage. Fibers broke near the edge of the dies at the maximum stress and the displacement increased at a constant high stress owing to progressive fiber breakage. Most fibers broke with further indentation and the stress decreased abruptly. The shear stress subsequently decreased gradually owing to the load bearing of the remaining fibers, such as burrs on the lateral sides.

[insert Figure 3]

The specimens were removed from the jig during the test and observed using an optical microscope (Fig. 4). The specimens evaluated before reaching the maximum stress exhibited slight plastic deformation (Fig. 4a). Some fiber breaks were observed at random positions in the shearing (clearance) zone. Major cracks (progressive fiber breaks) appeared on the top and bottom surfaces after the maximum stress was reached and these cracks extended gradually in

the through-thickness direction (Fig. 4b). The matrix dropped off and the fibers fuzzed in the region close to the failure surface (Fig. 4c). When the strain field was measured using the two-dimensional digital image correlation technique at half of the maximum stress, the shear strain exceeded 5% in the narrow shearing zone. The shear strain thus reached 10% at the maximum stress and the matrix and fiber/matrix interface in the shearing zone also failed at such a high shear strain.

[insert Figure 4]

Table 2 and Fig. 5 present the relationship between the maximum shear stress and clearance. The maximum shear stress increased linearly with decreasing clearance. The shear strength of fiber failure of the CFRP unidirectional laminates was estimated to be approximately 350 MPa from the intercept of zero clearance. As stress concentration occurred at the tip of the loading dies, the actual shear strength would be higher than the estimated value. To assess the shear strength of carbon fibers, the damage states of the matrix and fiber/matrix interface at the maximum stress level should be observed in detail to evaluate the load carrying ability.

[insert Table 2 and Figure 5]

Furthermore, in the punch-tool shear test [24], the maximum shear stress of a specimen with fibers inclined slightly in the through-thickness direction was higher than that of a specimen with an in-plane fiber orientation. This result is probably due to the reorientation of fibers, so

the influence of large shear deformation must be considered for the quantitative evaluation of shear strength.

3.2 Damage accumulation in cross-ply laminates owing to out-of-plane shearing

The breakage of fibers owing to out-of-plane shear loading indicated that the CFRP laminates could be cut using shearing. Shearing, also known as die cutting, is used commonly in metal processing for mass production owing to its high machining speed. However, there have been only a few studies that aimed to cut FRPs by out-of-plane shearing [26] or similar machining methods such as punch shearing [27] and fine blanking [28,29]. The process of damage accumulation during shear cutting has not yet been clarified and the important machining factors have not been determined. Consequently, severe machining damage has been reported under certain conditions [27]. In this study, out-of-plane shear tests of cross-ply laminates were performed and the processes of damage accumulation and cutting were investigated to discuss the feasibility of the out-of-plane shearing of CFRP laminates.

Coupon specimens were prepared as mentioned in Section 2, and the stacking sequence of the laminates was $[0_2/90_2]_S$ and $[0/90]_{2S}$. The specimen was fixed on the jig (Fig. 1) and the 10-mm part of the specimen was cut by out-of-plane shear loading under some clearance conditions (0.01-0.50 mm). The crosshead speed was 0.5 mm/min. Additionally, specimens were removed from the jig during the test to optically observe the process of damage accumulation from the

edges. Moreover, delamination was observed by soft X-ray radiography (M-100, Softex).

Figure 6 presents the shear stress–displacement curves of $[0_2/90_2]_S$ laminates. The relationship between the maximum stress and clearance is presented in Table 2 and Fig. 5 along with that of $[0_8]$ unidirectional laminates. The maximum stress of the cross-ply laminates was 50 MPa lower than that of the unidirectional laminates under all the clearance conditions. This is attributed to the damage in the laminate. Figure 7 illustrates the edge observations during the tests. Micro-cracks in the 90° ply and delamination in the shear zone appeared first and grew with further indentation. Figures 7a and 7b suggest that the delamination was caused by interlaminar shear deformation, but not by matrix cracks and fiber breakage. The upper 0° ply broke at the edge of the die and the shear stress decreased abruptly, but most of the bottom 0° ply remained at this stage (Fig. 7c). The shear stress decreased gradually owing to the subsequent breakage of the bottom 0° ply (Fig. 7d). The cutting lines of the 0° plies and 90° ply were not aligned and the fixed side coupon exhibited a step-like failure surface (Fig. 7e). Little delamination remained in the fixed side coupon.

[insert Figures 6 and 7]

Figure 8 illustrates the edge observation of the fixed side coupon of a $[0/90]_{2S}$ laminate after the test. The cutting line from the bottom surface did not coincide with that from the top surface, similar to the $[0_2/90_2]_S$ laminate. Delamination remained at the interface between the second top 90° ply and third 0° ply. Figures 7 and 8 indicate that delamination was generated by the

high shear stress used to cut the carbon fibers and it remained in the fixed side after complete cutoff. Table 3 and Fig. 9 present the delamination area remaining in the fixed side coupon observed using soft X-ray radiography. The delamination area decreased with decreasing clearance and the average delamination length, which is equal to the area divided by the width (10 mm), was approximately 0.2 mm in both cross-ply laminates. This result indicated that the delamination extended only into the narrow shearing zone even in the thermoset CFRP laminates in which delamination likely occurs.

[insert Figure 8, Table 3 and Figure 9]

In general, the machining time of shearing is considerably short, and this is the advantage of the machining method for mass production. However, a step-like cut surface and delamination were observed. It is necessary for a machining method to optimize parameters such as the shape of the die, clearance, cutting speed, and temperature [27,30]. As high shear stress is inevitable at the ply interfaces, the work material should be limited to tough woven laminates and fiber-reinforced thermoplastics (FRTPs) to prevent delamination.

4. Concluding remarks

Shear-induced fiber failure of CFRP unidirectional laminates was investigated using out-of-plane shear tests. The maximum shear stress of fiber failure was much higher than the shear strength of matrix failure, which was measured using several standard shear test methods for

composite laminates. The maximum shear stress observed to induce progressive fiber failure at zero clearance was estimated to be 350 MPa for the unidirectional CFRP laminates used. A detailed analysis of the out-of-plane shearing is required for the quantitative evaluation of the shear strength; this analysis must consider the stress concentration at the tip of loading dies, the large deformation of the specimen, and the state of the matrix at the final failure.

The unidirectional laminates were cut by out-of-plane shear loading without severe damage, which suggests the possibility of using this loading pattern as a machining method for CFRP laminates. The out-of-plane shear tests of cross-ply laminates were subsequently carried out to clarify the process of damage accumulation and complete cutoff. Delamination appeared in the narrow shear zone before the onset of fiber failure and it remained in the fixed side coupon after complete cutoff. However, the average delamination length was 0.2 mm even in the thermoset CFRP laminates in which delamination likely occurs. The generation of delamination will be prevented in tough woven laminates and FRTPs after optimizing the machining parameters such as the die shape, clearance, and temperature.

Appendix. Tensile tests of unidirectional laminates with small off-axis angles

In the tensile tests of off-axis unidirectional laminates, fiber failure was observed at a small fiber orientation angle, and matrix failure appears at most orientation angles. It is well known that the off-axis tensile strength can be predicted using the Tsai–Hill criterion. In this section,

the shear strength of unidirectional laminates is investigated for small off-axis angles, although the in-plane shear stress contributes to failure in this test. CFRP laminates (T700S/#2592, Toray Industries) were used and the laminates were fabricated according to the procedure described in Section 2. Each specimen had a length of 160 mm, width of 10 mm, and thickness of 0.28 mm with a lamination of [θ_2] to avoid misalignment. The fiber orientation angle θ was varied in the range of 0°–9°. Specimens with θ = 30°, 45°, 60°, and 90° were also prepared to clarify the overall behavior of the tensile strength as a function of θ. Oblique end-tabs [31] made of GFRP were attached to alleviate the stress concentration near the grips. The specimens were loaded in tension using a universal testing machine (AG-50kNXplus, Shimadzu) at a crosshead speed of 0.5 mm/min. Five specimens were tested for each orientation.

Figure 10a presents a plot of the tensile strength against the orientation angle. The prediction according to the Tsai–Hill criterion, represented by the following equation, is consistent with the test results.

$$\sigma_{off-axis} = 1/\sqrt{\frac{\cos^2\theta(\cos^2\theta-\sin^2\theta)}{F_L^2}+\frac{\sin^4\theta}{F_T^2}+\frac{\cos^4\theta}{F_S^2}} \quad (1)$$

F_L and F_T are the measured strengths at θ = 0° and 90°, and the shear strength, F_S (=60 MPa), was estimated by fitting the prediction to the test results. Within the angle range $\theta \leq 9°$, the transverse stress term can be omitted from the Tsai–Hill criterion, as the value of $\sin^2\theta$ is sufficiently small. In this case, the failure criterion becomes the elliptical equation of the longitudinal stress σ_{11} and shear stress τ_{12}.

$$\left(\frac{\sigma_{11}}{F_L}\right)^2 + \left(\frac{\tau_{12}}{F_S}\right)^2 = 1 \quad (2)$$

Figure 10b presents the relationship between σ_{11} and τ_{12} of all the specimens at final failure, which were calculated using the transformation of the stress components. Equation (2) is consistent with the experiment results within $\theta \geq 3°$, where the matrix failed. However, Eq. (2) with a shear strength of 60 MPa deviated from the results within the range $0.5° \leq \theta \leq 2°$. This suggested that the contribution of the shear stress to fiber failure cannot be evaluated using the shear strength of matrix failure.

[insert Figure 10]

References

[1] Gordon S and Hillery MT. A review of the cutting of composite materials. *Proc Inst Mech Eng Part L* 2003; 217: 35-45.

[2] Soussia AB, Mkaddem A and Mansori ME. Rigorous treatment of dry cutting of FRP – Interface consumption concept: A review. *Int J Mech Sci* 2014; 83: 1-29.

[3] Wang XM and Zhang LC. An experimental investigation into the orthogonal cutting of unidirectional fibre reinforced plastics. *Int J Mach Tool Manuf* 2003; 43: 1015-1022.

[4] Xu W and Zhang L. Mechanics of fibre deformation and fracture in vibration-assisted cutting of unidirectional fibre-reinforced polymer composites. *Int J Mach Tool Manuf* 2016; 103: 40-52.

[5] Dandekar CR and Shin YC. Modeling of machining of composite materials: A review. *Int*

J Mach Tool Manuf 2012; 57: 102-121.

[6] Che D, Saxena I, Han P, et al. Machining of carbon fiber reinforced plastics/polymers: A literature review. *J Manuf Sci Eng* 2014; 136: 034001.

[7] Shetty N, Shahabaz SM, Sharma SS and Shetty SD. A review on finite element method for machining of composite materials. *Compos Struct* 2017; 176: 790-802.

[8] Abena A, Soo SL and Essa K. Modelling the orthogonal cutting of UD-CFRP composites: Development of a novel cohesive zone model. *Compos Struct* 2017; 168: 65-83.

[9] Gao C, Xiao J, Xu J and Ke Y. Factor analysis of machining parameters of fiber-reinforced polymer composites based on finite element simulation with experimental investigation. *Int J Adv Manuf Technol* 2016; 83: 1113-1125.

[10] Xu W, Zhang LC and Wu Y. Elliptic vibration-assisted cutting of fibre-reinforced polymer composites: Understanding the material removal mechanisms. *Compos Sci Technol* 2014; 92: 103-111.

[11] Iliescu D, Gehin D, Iordanoff I, et al. A discrete element method for the simulation of CFRP cutting. *Compos Sci Technol* 2010; 70: 73-80.

[12] Dandekar CR and Shin YC. Multiphase finite element modeling of machining unidirectional composites: prediction of debonding and fiber damage. *J Manuf Sci Eng* 2008; 130: 051016.

[13] Rao GVG, Mahajan P and Bhatnagar N. Micro-mechanical modeling of machining of FRP

composites – cutting force analysis. *Compos Sci Technol* 2007; 67: 579-593.

[14] Usui S, Wadell J and Marusich T. Finite element modeling of carbon fiber composite orthogonal cutting and drilling. *Procedia CIRP* 2014; 14: 211-216.

[15] Santiuste C, Soldani X and Miguélez MH. Machining FEM model of long fiber composites for aeronautical components. *Compos Struct* 2010; 92: 691-698.

[16] Rao GVG, Mahajan P and Bhatnagar N. Three-dimensional macro-mechanical finite element model for machining of unidirectional-fiber reinforced polymer composites. *Mater Sci Eng A* 2008; 498: 142-149.

[17] King TR, Blackketter DM, Walrath DE and Adams DF. Micromechanics prediction of the shear strength of carbon fiber/epoxy matrix composites: the influence of the matrix and interface strengths. *J Compos Mater* 1992; 26: 558-573.

[18] Ghafarizadeh S, Chatelain J-F and Lebrun G. Finite element analysis of surface milling of carbon fiber-reinforced composites. *Int J Adv Manuf Technol* 2016; 87: 399-409.

[19] Feito N, López-Puente J, Santiuste C and Miguelez MH. Numerical prediction of delamination in CFRP drilling. *Compos Struct* 2014; 108: 677-683.

[20] Phadnis VA, Makhdum F, Roy A and Silberschmidt VV. Drilling in carbon/epoxy composites: Experimental investigations and finite element implementation. *Compos Part A* 2013; 47: 41-51.

[21] Isbilir O and Ghassemieh E. Numerical investigation of the effects of drill geometry on

drilling induced delamination of carbon fiber reinforced composites. *Compos Struct* 2013; 105: 126-133.

[22] Isbilir O and Ghassemieh E. Finite element analysis of drilling of carbon fibre reinforced composites. *Appl Compos Mater* 2012; 19: 637-656.

[23] Crescenzi F, Marini F, Nardi C, et al. Mechanical characterization of glass fibre–epoxy composite material for ITER pre-compression rings. *Fusion Eng Des* 2011; 86: 2553-2556.

[24] Formisano A, Boccarusso L, Durante M and Langella A. Punch tool based out-of-plane shear behaviour of GFRP composites. *Compos Struct* 2017; 163: 325-330.

[25] Liu K and Piggott MR. Shear strength of polymers and fibre composites: 1. Thermoplastic and thermoset polymers. *Composites* 1995; 26: 829-840.

[26] Tatsuno D, Yoneyama T, Kawamoto K and Okamoto M. Production system to form, cut, and join by using a press machine for continuous carbon fiber-reinforced thermoplastic sheets. *Polym Compos*; DOI: 10.1002/pc.24242 (in press).

[27] Klocke F, Shirobokov A, Kerchnawe S, et al. Experimental investigation of the hole accuracy, delamination, and cutting force in piercing of carbon fiber reinforced plastics. *Procedia CIRP* 2017; 66: 215-220.

[28] Baskaran G, Gowri S and Krishnamurthy R. Study on vital static properties of fine blanking of GFRP composites with that of conventional drilling. *Int J Adv Manuf Technol* 2010; 50: 659-666.

[29] Zal V, Naeini HM, Bahramian AR and Abbaszadeh B. Experimental evaluation of blanking and piercing of PVC based composite and hybrid laminates. *Adv Manuf* 2016; 4: 248-256.

[30] Nakamura N, Ogi K, Ota A, et al. Shear cutting behaviors in thermosetting and thermoplatic CFRP laminates. *Key Eng Mater* 2015; 656-657: 347-352.

[31] Sun CT and Chung I. An oblique end-tab design for testing off-axis composite specimens. *Composites* 1993; 24: 619-623.

Figure captions

Figure 1 Experimental setup of the out-of-plane shear test.

Figure 2 Test results of the transverse (90°) specimens.

Figure 3 Shear stress–displacement curves of the longitudinal (0°) specimens tested under some clearances.

Figure 4 Edge observation of the longitudinal (0°) specimen tested under clearance of 0.05 mm; these micrographs correspond to the loading stage indicated in Fig. 3.

Figure 5 Relationship between the maximum shear stress and clearance. Each point represents the average value of the five specimens and the error bar indicates the maximum and minimum values.

Figure 6 Shear stress–displacement curves of the cross-ply $[0_2/90_2]_S$ laminates under some clearances.

Figure 7 Edge observation of the cross-ply $[0_2/90_2]_S$ laminates tested under the clearance of 0.05 mm; these micrographs correspond to the loading stage designated as (a)–(e) in Fig. 6.

Figure 8 Observation of the cross-ply $[0/90]_{2S}$ laminate tested under the clearance of 0.05 mm

Figure 9 Change in the delamination area with the clearance. Delamination was observed using soft X-ray radiography.

Figure 10 Results of the off-axis tensile tests of unidirectional laminates.

Table captions

Table 1 Strength properties used in the machining simulations.

Table 2 Measured maximum shear stress against the clearance.

Table 3 Measured projection area of the delamination against the clearance.

Table 1 Strength properties used in the machining simulations.

(a) Properties of carbon fibers for the micro-mechanical model of orthogonal cutting

Longitudinal tensile strength (MPa)	3590	2678	2000	3200	3600	3590
Longitudinal compressive strength (MPa)	3000			2000		350
Transverse tensile strength (MPa)						1800
Transverse compressive strength (MPa)						2730
Shear strength (MPa)			380 *1		38	380 *1
Reference No.	[8]	[9]	[10]	[11] *2	[12]	[13]

*1 Shear strength used in the finite-element program WYO2D [17].

*2 Fiber model by the discrete element method (DEM)

(b) Properties of a unidirectional CFRP for the equivalent homogeneous model of orthogonal cutting

Longitudinal tensile strength (MPa)	2510	1950	2280
Longitudinal compressive strength (MPa)	1682	1480	1725
Transverse tensile strength (MPa)	27	48	57
Transverse compressive strength (MPa)	27	200	228
In-plane shear strength (MPa)		79	76 (τ_{12})
			46 (τ_{13})
Transverse shear strength (MPa)			52 (τ_{23})
Reference No.	[14]	[15]	[16]

(c) Properties of a unidirectional CFRP for the equivalent homogeneous model of drilling

Longitudinal tensile strength (MPa)	1388	2720	2720	1900	1900
Longitudinal compressive strength (MPa)	551.69	1690	1690	1000	1000
Transverse tensile strength (MPa)	48.2		111	84	84
Transverse compressive strength (MPa)	124.53	214	214	250	250
In-plane shear strength (MPa)	76.75	115	115	60 (τ_{12})	110 (τ_{12})
				110 (τ_{13})	
Transverse shear strength (MPa)	45.9			110 (τ_{23})	
Reference No.	[18]	[19]	[20]	[21]	[22]

Table 2 Measured maximum shear stress against the clearance.

Clearance (mm)	Maximum shear stress (MPa)	
	$[0_8]$	$[0_2/90_2]_S$
0.05	334.3	297.8
0.1	317.0	269.9
0.2	302.0	229.0
0.5	198.4	153.2

Table 3 Measured projection area of the delamination against the clearance.

Clearance (mm)	Projected delamination area (mm^2)	
	$[0_2/90_2]_S$	$[0/90]_{2S}$
0.01		1.92
0.02		1.47
0.03		1.55
0.04		1.49
0.05	2.61	1.59
0.06		1.33
0.07		1.68
0.08		1.39
0.09		1.52
0.1	2.87	3.16
0.2	3.32	
0.5	5.38	

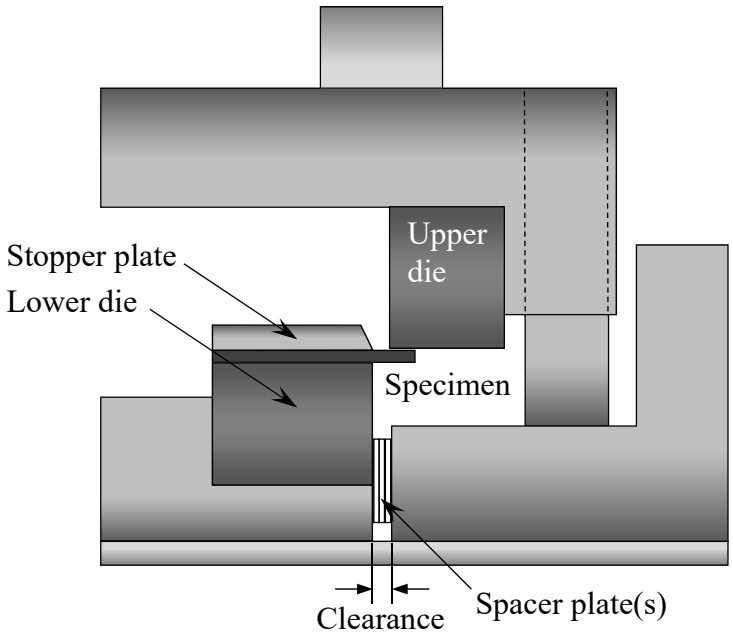

Fig. 1 Schematic of the jig used in the out-of-plane shear test.

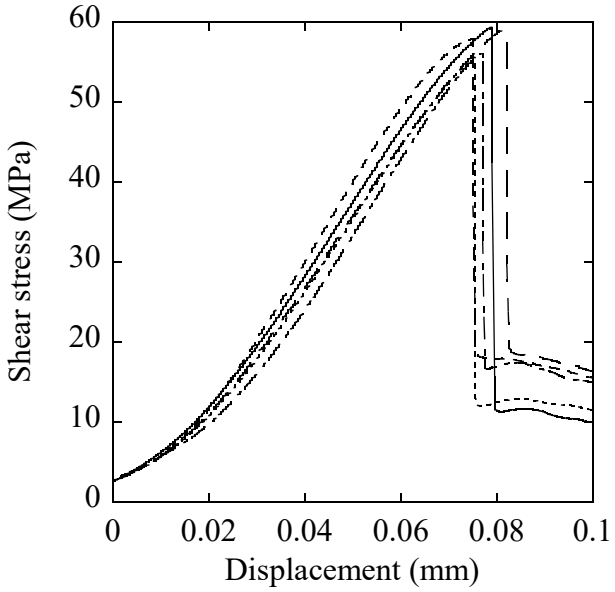

(a) Shear stress-displacement curves

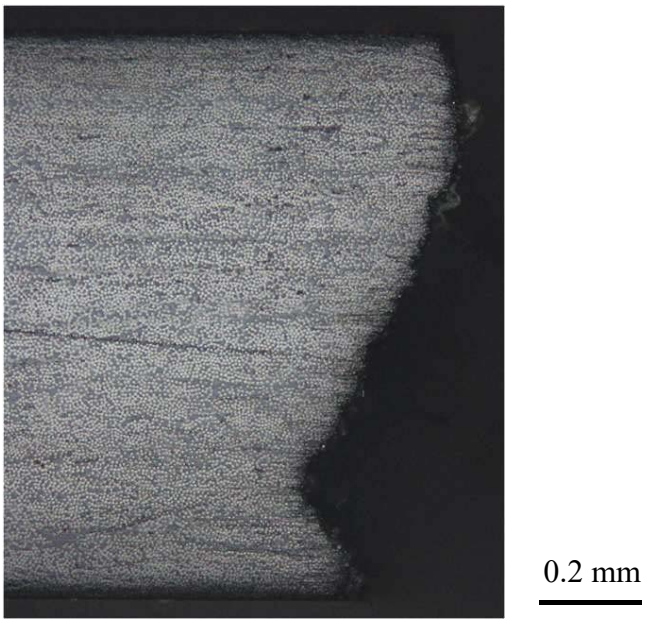

(b) Optical micrograph of the edge

Fig. 2 Test results of the transverse (90º) specimens.

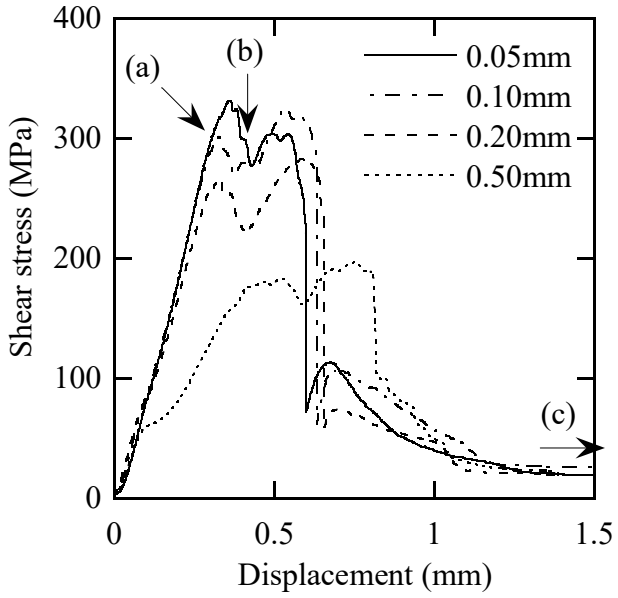

Fig. 3 Shear stress-displacement curves of the longitudinal (0º) specimens tested under some clearances.

(a) Before the maximum stress

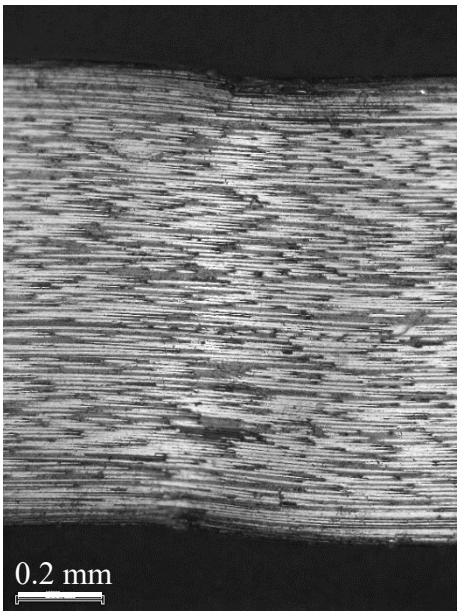

(b) After the maximum stress

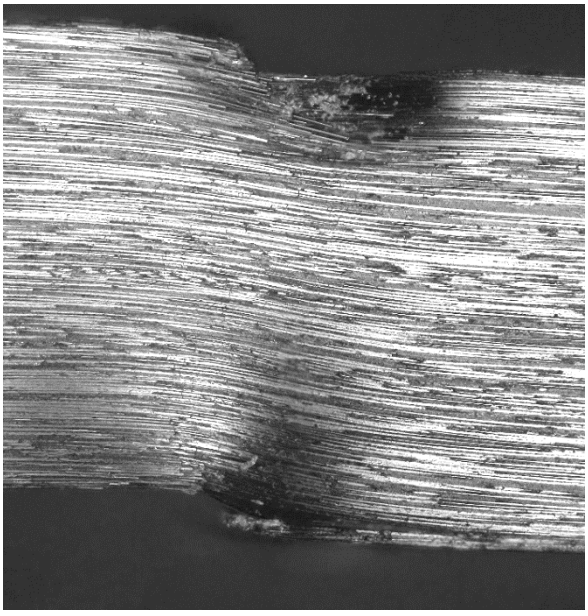

(c) After final failure

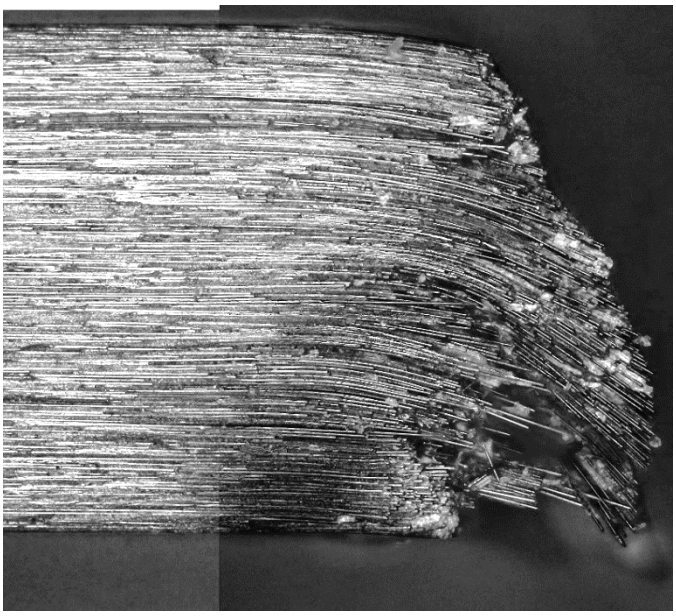

Fig. 4 Edge observation of the longitudinal (0º) specimen tested under 0.05-mm clearance; these micrographs correspond to the loading stage indicated in Fig. 3.

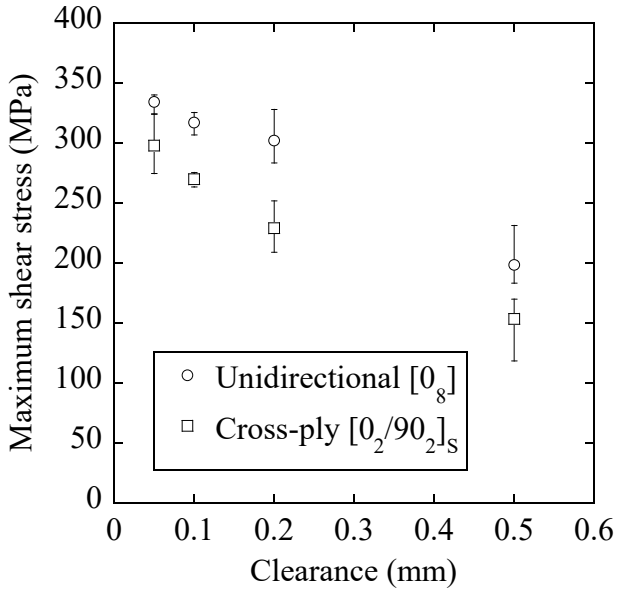

Fig. 5 Relationship between the maximum shear stress and the clearance. A point is the average of the five specimens and the error bar indicated the maximum and minimum values.

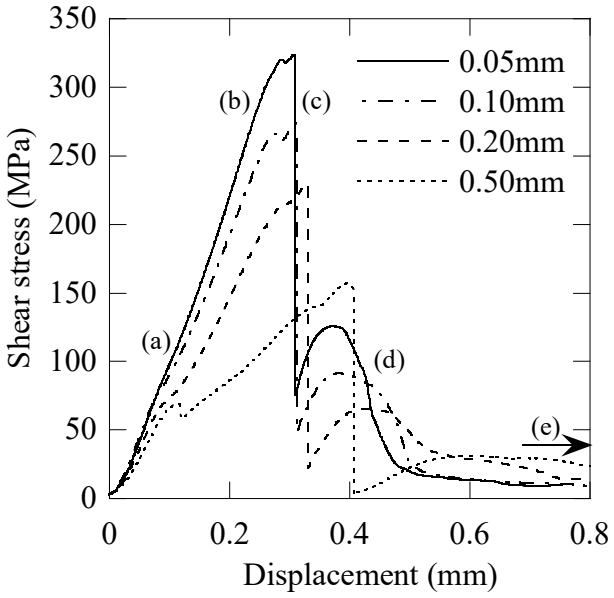

Fig. 6 Shear stress-displacement curves of the cross-ply $[0_2/90_2]_S$ laminates under some clearances.

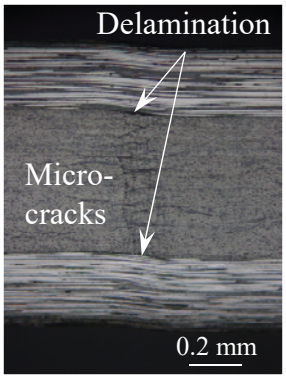

(a) After slight change in slope

(b) Before reaching the maximum stress

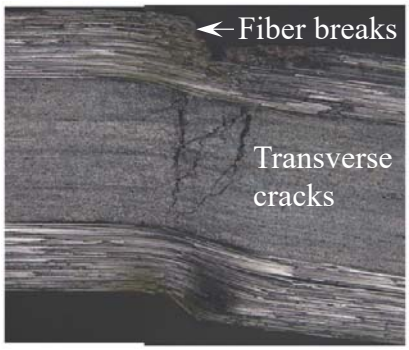

(c) Just after abrupt stress drop

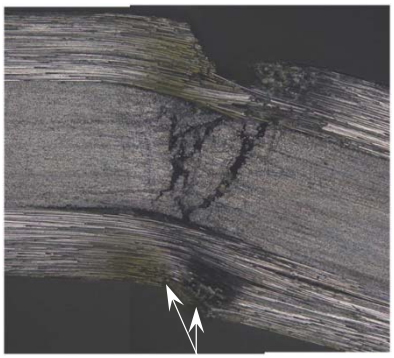

(d) During gradual stress reduction

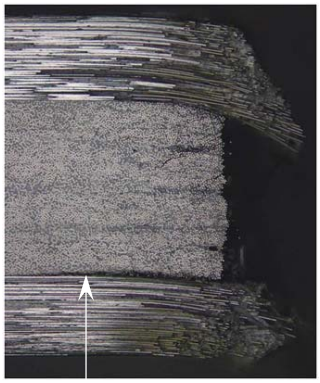

(e) After complete cutoff

Fig. 7 Edge observation of the cross-ply $[0_2/90_2]_S$ laminates tested under 0.05-mm clearance; these micrographs correspond to the loading stage designated as (a)-(e) in Fig. 6.

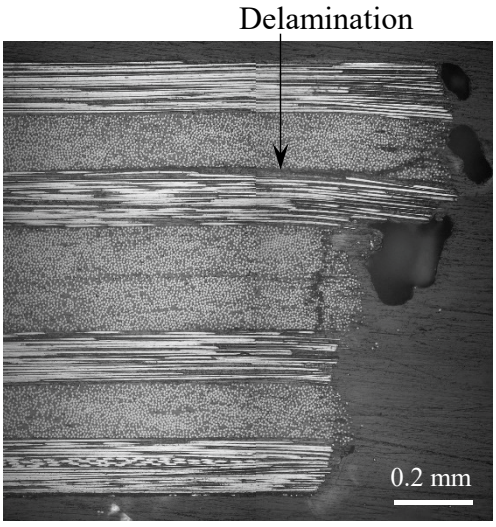

Fig. 8 Observation of the cross-ply $[0/90]_{2S}$ laminate tested under 0.05-mm clearance.

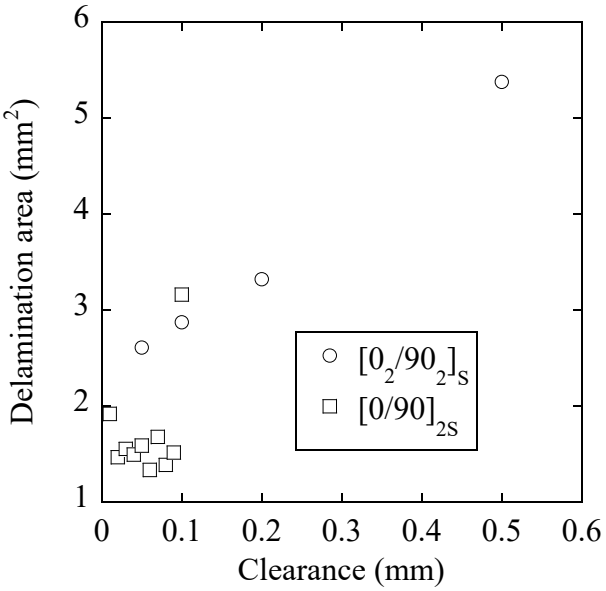

Fig. 9 Change in the delamination area by the clearance. Delamination was observed by soft X-ray radiography.

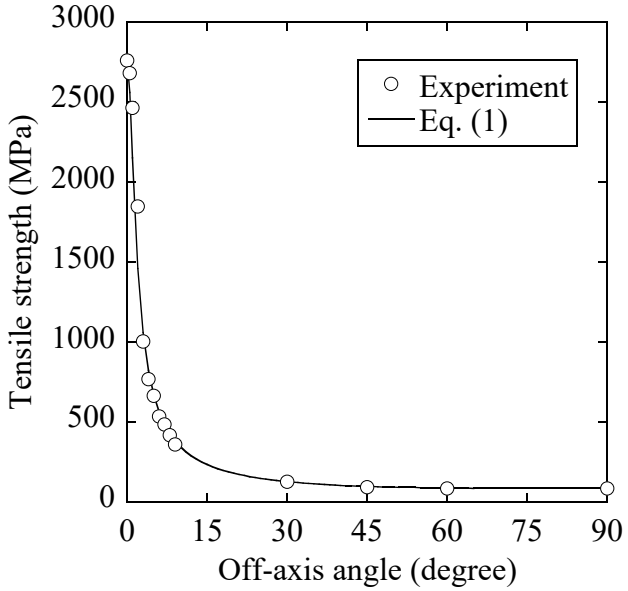

(a) Off-axis tensile strength

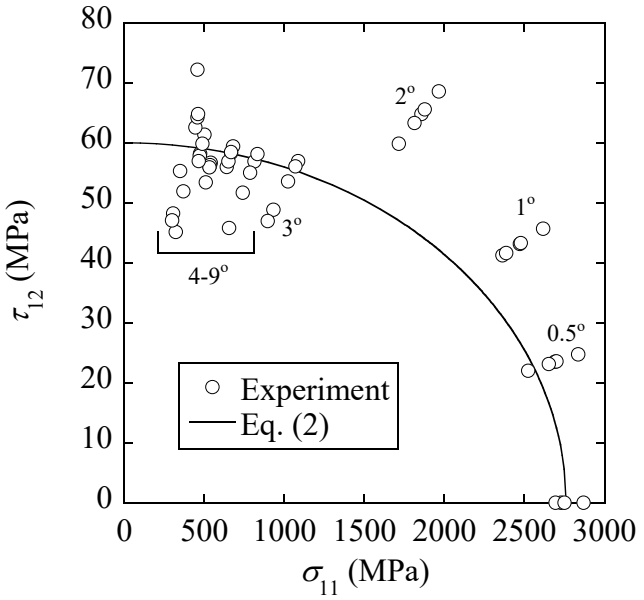

(b) Calculated stress components at failure

Fig. 10 Results of the off-axis tensile tests of unidirectional laminates.